43rd AIAA Aerospace Sciences Meeting and Exhibit
10 - 13 January 2005, Reno, Nevada

AIAA 2005-963

Modeling of Thermal Transpiration Flows for Knudsen Compressor Optimization

A. A. Alexeenko, S. F. Gimelshein, and E. P. Muntz
University of Southern California, Los Angeles, CA 90089

Andrew Ketsdever
Air Force Research Laboratory, Propulsion Directorate, Edwards AFB, CA 93524

Abstract

Rarefied gas flows through two-dimensional finite length capillaries are studied numerically with the goal of performance optimization of a nanomembrane-based Knudsen compressor. Both density and temperature gradient driven flows are considered in a wide range of Knudsen numbers from 0.05 to 75. The length-to-height ratios from 5 to 30 were examined. Three different wall temperature distributions were considered, namely, linear, step-wise, and a non-monotonic profile typical for a radiantly heated Knudsen compressor membrane. The direct simulation Monte Carlo method was used for shorter channels, and a discrete ordinate method for the solution of the BGK model equation is utilized for a longer channel. The mechanism for the Knudsen minimum in flow conductance is quantitatively explained, the short channel end effects are characterized, and the sensitivity of the mass flow rate to a non-monotonic temperature distribution is shown.

1 Introduction

Lab on a chip technology is drawing the attention of scientists from many disciplines. Recent advances in MEMS manufacturing have made it possible to construct microscale analytical sensors such as integrated gas chromatography systems, miniature spectrometers, and mass spectrometers. The miniaturized detection devices will require microscale roughing pumps to provide sensor elements with gas samples at necessary environmental conditions. A pumping mechanism that can be exploited at microscale is thermal transpiration, a rarefied gas effect that drives the gas flow along the temperature gradient in a tube or channel. The main goal of this paper is the numerical study of thermal transpiration flows in short microchannels to aid in the performance optimization of a transpiration based microscale roughing pump known as the Knudsen compressor [1].

In early 1900s M. Knudsen built and studied the first transpiration based compressor, consisting of a series of differentially heated and cooled capillaries. Each stage of the compressor had a capillary section where the wall temperature increases, causing a thermomolecular pressure build-up at the high-temperature end of the capillary. The capillaries are followed by a connector stage of a significantly larger cross-sectional area, where the pressure is almost constant and temperature is decreased to its original value at the beginning of the stage. The modern version of Knudsen compressor was suggested by Pham-Van-Diep *et al*[2] and demonstrated by Vargo and Muntz[3]. The most critical element of the Knudsen compressor developed at USC is the thermal transpiration membrane made of porous materials, such as aerogel, with pore diameters on the order of the mean free path of the gas at standard atmospheric conditions. The temperature gradient is maintained across the transpiration membrane by resistive or radiant heating. Recently, a single-chip micromachined implementation of a Knudsen pump was reported in Ref. [4], which can evacuate a cavity to 0.46 atm while operating at atmospheric pressure and using 80mW input power.

Knudsen compressor has several attractive fea-

Report Documentation Page

Form Approved
OMB No. 0704-0188

1. REPORT DATE	2. REPORT TYPE	3. DATES COVERED
JAN 2005		**-**

4. TITLE AND SUBTITLE	5a. CONTRACT NUMBER
The Modeling of Thermal Transpiration Flows for Knudsen Compressor Optimization	5b. GRANT NUMBER
	5c. PROGRAM ELEMENT NUMBER

6. AUTHOR(S)	5d. PROJECT NUMBER
A Alexeenko; S Gimelshein; E Muntz; A Ketsdever	**2308**
	5e. TASK NUMBER **0532**
	5f. WORK UNIT NUMBER

7. PERFORMING ORGANIZATION NAME(S) AND ADDRESS(ES)	8. PERFORMING ORGANIZATION REPORT NUMBER
Air Force Research Laboratory (AFMC),AFRL/PRSA,10 E. Saturn Blvd.,Edwards AFB,CA,93524-7680	

9. SPONSORING/MONITORING AGENCY NAME(S) AND ADDRESS(ES)	10. SPONSOR/MONITOR'S ACRONYM(S)
	11. SPONSOR/MONITOR'S REPORT NUMBER(S)

12. DISTRIBUTION/AVAILABILITY STATEMENT
Approved for public release; distribution unlimited

13. SUPPLEMENTARY NOTES

14. ABSTRACT
Rarefied gas flows through two-diensional finite length capillaries are studied numerically with the goal of perfoirmance oiptimization of a nanomembrane-based Knudsen compressor. Both density and temperature gradient driven flows are considered in a wide range of Knudsen numbers from 0.05 to 75. The length-to-height ratios from 5 to 30 were examined. Three different wall temperature distributions were considered, namely, linear, step-wise, and a non-monotonic profile typical for a radiantly heated Knudsen compressor membrane. The direct simulation Monte Carlo method was used for shorter channels, and a discrete ordinate method for the solution of the BGK model equation is utilized for a longr channel. The mechanism for the Knudsen minimum in flow conductance is quantitatively explained, the short channel end effects are characterized, and the sensitivity of the mass flow rate to a non-monotonic temperature distribution is shown.

15. SUBJECT TERMS

16. SECURITY CLASSIFICATION OF:			17. LIMITATION OF ABSTRACT	18. NUMBER OF PAGES	19a. NAME OF RESPONSIBLE PERSON
a. REPORT	b. ABSTRACT	c. THIS PAGE			
unclassified	**unclassified**	**unclassified**		**11**	

tures, such as no moving parts and no fluids or lubricants, and therefore, can have a number of promising applications provided that its performance can be optimized to meet the existing pumping requirements. The two most important performance parameters of the compressor are the energy use and volume per unit throughput. To accomplish minimization of these performance parameters the Knudsen compressor must also be designed to maximize the gas conductance through the device for a given temperature change. The required flow rate in the Knudsen compressor can be obtained by adjusting the cross-sectional area of the stages and the temperature distribution along the transpiration membrane at different stages. The main element of the transpiration based pump is rarefied gas flow through a capillary.

Rarefied gas flows of different gases through long tubes and channels were a topic of an extensive experimental and theoretical research over several decades, and a comprehensive review of the numerical data and analytical results for rarefied gas flows in capillaries was performed by Sharipov and Seleznev[5] (see also references therein). There is however a lack of reference data for nonisothermal flow through a capillary of a finite length, especially for arbitrary pressure and temperature drops.

The present numerical modeling of thermal transpiration flows in microchannels addresses several questions important for design optimization of Knudsen compressors, namely: the influence of different temperature internal distributions across the membrane on the flow field inside the capillaries and the total transpiration mass flow rates, the impact of the rarefaction on the capillary throughput, and capillary end effects.

2 Scope of Simulations

In the present work, two reservoirs filled with a single-species gas and joined by a two-dimensional capillary of a finite length L and height h are considered in the computations. The two-dimensional configuration corresponds to the case of a capillary of infinite width w. A schematic of the geometric configuration and notations used throughout this paper are shown in Fig. 1. The subscripts I and II refer to the quantities attributed to the left and right container, respectively (far enough from the channel inlet and outlet). The channel walls have some temperature distribution varying from T_I to T_{II}. If the reservoirs are at the same temperature ($T_I = T_{II}$) and the pressure p_I is larger than p_{II} there will be a mass flow from the left container to the right one. Conversely, if the pressures are equal but a temperature drop is maintained between the reservoirs then the gas flow develops from the cold container to the hot one.

The summary of cases that have been considered for two-dimensional channel flows is given in Table 1. The gas is molecular nitrogen in all simulations. The first set of computations is for a pressure-driven flow in finite length channels for a range of Knudsen numbers from near-continuum to free molecular (cases I-a to I-e). Hereafter, the Knudsen number is based on the mean free path in the right reservoir and the channel height. Note also that the change in Knudsen number is due a change in the mean free path and not the channel geometry. A second set includes cases II-a to II-e that correspond to a flow with both pressure and temperature gradients in a channel with a length-to-height ratio of 5. For each of these five cases we consider two different wall temperature distributions: linear and step-wise. Finally, the influence of different wall temperature distributions is examined in a channel that connects reservoirs with a temperature ratio $T_I/T_{II} = 2$ and zero pressure drop (cases III-a to III-c).

2.1 DSMC Method

The DSMC method [6] has been applied in this work to obtain numerical solutions for short microchannel flows. The DSMC method is a numerical approach to model gas flows in a wide range of Knudsen numbers from the near continuum to free molecular flow regimes. The DSMC-based software SMILE [7] is used for all DSMC computations. The code uses the majorant frequency scheme [8] of the DSMC method for modeling of collisional process. The intermolecular potential is assumed to be the variable soft sphere model [9]. The Larsen-Borgnakke model[10] with temperature-dependent Z_r and Z_v and discrete rotational and vibrational energies is used for the energy exchange between the translational and internal modes. At the gas-wall interface the the Maxwell model is used with the fully diffuse accommodation of tangential momentum and energy.

2.2 BGK Model Kinetic Equation Solution

The computational cost of DSMC simulations of low-speed flows in long channels becomes prohibitive due to low signal-to-noise ratio[11]. This is why for modeling of such flows it is reasonable to

consider the solution of the steady-state Boltzmann equation with the collision operator simplified using BGK model[12],

$$U\frac{\partial f}{\partial x} + V\frac{\partial f}{\partial y} = \nu(f_0 - f) \tag{1}$$

where $f(x, y, U, V, W)$ is the distribution function, x and y are Cartesian coordinates, U, V, W are velocity components, ν is the collision frequency and f_0 is the local equilibrium Maxwell-Boltzmann distribution function which depends on the moments of the distribution function f. This is a non-linear integrodifferential equation that uses a simplified form of the collision integral compared to the Boltzmann equation, and is applicable to model gas flows with arbitrary Knudsen numbers and degree of flow nonequilibrium.

The BGK model kinetic equation can be solved using a finite-difference method and standard discrete-ordinate method procedures [13] for interpolation of the distribution function in velocity space. The velocity components (U, V) are transformed into polar coordinates (S, ϕ). The Gauss-Hermite half range quadrature [14] of order 16 and three-eights rule are used for integration over the speed and velocity angle, respectively.

3 Results and Discussion

3.1 Pressure-Driven Flow in Short Channels

First consider the pressure-driven flow in a short channel with a length-to-height ratio of 5. The DSMC solutions have been obtained for different Knudsen numbers from the near continuum to free molecular regime (cases I-a to I-e in Table 1). The ratio of the upstream to downstream reservoir pressures in these cases is 1.5.

The end effects in a short channel result in the effective elongation of the capillary which is clearly observed in Fig. 2 where the pressure profiles along X-axis are plotted for different Knudsen numbers. The pressure drop extends significantly beyond the channel inlet and outlet for all Knudsen number cases. The deviation of pressure from a linear profile is shown in Fig. 3. It is seen that such a deviation increases with Knudsen number and reaches a maximum of about 6% for Kn_{II}=50.

The calculated mass flow rates for Cases I-a to I-e are given in Table 4. The flow coefficients Q_P and Q_T are used here that are usually employed for characterization of the Poiseuille and thermal creep flows for the conditions of small temperature and pressure gradients. The flow coefficients are defined as follows:

$$Q_P = \frac{\dot{M}}{(\frac{1}{2}\sqrt{2RT_0})\rho_0 w h^2 \frac{1}{p_0}\frac{\Delta p}{L}} \tag{2}$$

$$Q_T = \frac{\dot{M}}{(\frac{1}{2}\sqrt{2RT_0})\rho_0 w h^2 \frac{1}{T_0}\frac{\Delta T}{L}} \tag{3}$$

where $\dot{M}$ is the mass flow rate (kg/s), ρ_0, p_0, and T_0 are the average density, pressure, and temperature, respectively, and w, h, L are channel width, height and length, respectively.

The calculated flow coefficient Q_P is plotted in Fig. 4 as a function of Knudsen number. There are also shown the flow coefficient Q_P for a Poiseuille flow between parallel plates[15] for small pressure differences and the flow coefficient Q_P for a short channel with L/h=5 in the free molecule regime [16]. As expected, the flow coefficient is larger for the longer channel due to the smaller influence of end effects on the mass flow. Note also that the computed free molecular values agree well with [16]. The difference between the computed flow coefficients and the one calculated in [15] becomes larger at large Knudsen numbers. The minimum in the flow coefficient observed at a Knudsen number of about 3 illustrate the well known Knudsen minimum effect.

The appearance of a conductance minimum observed by Knudsen has been qualitatively explained by Pollard and Present [17]. They suggested that at low pressure conditions, when the mean free path of the molecules is much greater than the height and the length of the channel, there are molecules that have near axial velocity components on entry to the channel or after a collision with the surface. These molecules tend to make a much larger contribution to the mass flow than other molecules. When pressure increases, the fraction of such molecules decreases since their paths are disrupted by molecular collisions. On the other hand, the molecular collisions generally tend to create a drift velocity that increases mass flow. Since the development of a drift velocity depends on the height-based Knudsen number, and the number of molecules that go straight through the channel depend on a the length-based Knudsen number, the impact of the decreasing molecular mean free path initially outweighs the drift velocity effect. As a result, the conductance initially decreases with Knudsen number, and therefore creates a minimum.

To quantitatively examine the Knudsen minimum effect, DSMC computations has been performed in a channel of a length-to-height ratio of 15 using

five chemically identical species. Species 1 and 4 are assigned to molecules that come from the upstream and downstream boundaries, respectively. When molecules of species 1 and 4 collide with the channel surface, they are transformed to species 2 and 5, respectively. Additionally, to study the effect of molecular collisions, species 3 is created from species 1 and 2 when they experience collisions with any other species inside the channel. Species 4 that collides with other molecules inside the channel, is transformed to species 5.

The distribution of mole fractions of these species along the centerline for Kn_{II}=75 is shown in Fig. 5. Here, the channel starts at X=0.005 m, and ends at X=0.020 m. Note first that although the population of molecules with no surface or molecular collisions (Species 1) decreases significantly through the channel, but still remains at about 1% at the exit. Species 1 is gradually replaced by species 2 and 3, with the former gradually decreasing along the channel, and latter reaching its maximum near the center. Note also that near the exit, the population of molecules that come from the upstream boundary decreases to about 10% due to the backscattering. The remaining 90% of molecules come from the downstream reservoir. The fraction of these molecules that travel upstream through the channel and reach the entrance is about 0.3% (Species 4). Consider now the contribution of different species into the total mass flow given in Table 2 along with their relative concentration. The important fact is that although the concentration of species 1 is about three times smaller than species 2, its contribution to the mass flow is only about two times smaller. Another important fact is that species 1 effectively contributes about 40% to the total mass flow, since the the contributions of species 3, 4, and 5 cancel out. That means that if species 1 had an X-velocity similar to those of species 2 and 3, the total mass flow would be almost 12% lower.

The results for a smaller Kn_{II}=1.5 are presented in Fig 6. The most important conclusion here is that no molecules cross the channel without collisions with other molecules. The mole fraction of species 1 and 2 at the channel exit and species 4 at the channel entrance are essentially zero. It is interesting to note that the fraction of upstream molecules reaching the exit is about 10%, similar to the larger Knudsen number case. Comparison of the species mass flows is shown in Table 3. Since the mass flow of species 4 increases 50 times as compared to Kn_{II}=75, same as the density does for these two cases, it is clear that there is no yet any drift velocity formed for Kn_{II}=1.5. The absence of a high-velocity contribution from species 1 explains therefore the Knudsen minimum, with the mass flow per pressure drop decreasing when the Knudsen number is reduced from 75 to 1.5. The computations also showed that a drift velocity begins to form at a Knudsen number of about 0.75.

The existence of the Knudsen minimum is illustrated in Fig. 7 where the mass flow per pressure drop is shown. The reduced mass flow is about 18% higher at Kn_{II}=75 than at Kn_{II}=1.5. About two thirds of this is due to molecules that cross the whole channel without gas and surface collisions, and the remaining part is due to molecules that after a collision with the surface acquire low radial and high axial velocity components. The computations also showed that the Knudsen minimum is observed not only for a relatively long channel of L/h=15, but also for a short channel with L/h=5. For the latter one the minimum amounts to only about 1.5%.

3.2 Pressure and Temperature Driven Flow in a Short Channel

In the above section, the flow of a gas driven by density gradients was considered in the absence of a temperature difference between reservoirs. The situation is often reversed in a Knudsen compressor nanomembrane flow, when the flow is primarily driven by temperature gradients. In order to study separately the temperature effect, a temperature drop is assumed across the channel, with the density in the reservoirs being equal. Such flows through finite length channels in the presence of both temperature and pressure differences are examined in this section. The presented results correspond to Cases II-a to II-e in Table 1. In all of the considered cases, the pressure ratio $P_I/P_{II} = 1.5$ and temperature ratio is T_I/T_{II}=1.5. Since the pressure ratio in these cases exceeds the thermomolecular pressure ratio, there is a non-zero mass flow from the left reservoir to the right one. For each set of reservoir conditions two different cases of temperature distribution are simulated, (1) a linear distribution from T_I to T_{II}, and (2) a step-wise distribution $T_w(x) = T_I$ for $x < L/2$; $T_w(x) = T_{II}$ for $x \geq L/2$.

The calculated X-component of the velocity field is shown in Fig. 8 for the Cases II-d and II-e that correspond to the Knudsen number of 0.2 and 0.05, respectively. The most important conclusion that may be drawn from these figures is that the temperature distribution does not impact the flow outside of the channels. This is true for both Knudsen num-

bers considered. Moreover, the velocity fields for the linear and step-wise temperature distributions are close near the surface, but differ significantly at the centerline.

Comparison of density profiles along the centerline for the above cases is given in Fig. 9. General behavior of density profiles is similar for different Knudsen numbers and temperature variation, with density being lower in the high-temperature part, and higher in the low-temperature part. This is related to a relatively lower thermal velocities of the latter and, as the result, their longer residence time and larger densities. Similarly, the population of molecules in the high temperature region is affected by short residence times in that region. This effect is obviously more pronounced in the step distribution cases. The molecular collisions increase the deviation of density from its average value.

The X-component of velocity profile along the centerline is plotted in Fig. 10. The pressure-driven Poiseuille and temperature-driven thermal creep flows represent two competing flow mechanisms in these cases. Due to the thermal creep flow from the cold container to the hot one, the X-component of velocity is lower in Cases II-e (lin) and II-e (step) than in Case I-e. In the case of step-wise wall temperature distribution, the resulting velocity profile in the channel is non-monotonic, and has a strong gradient in the step region due to thermal creep.

3.3 Influence of Wall Temperature Distribution

The influence of wall temperature distribution on the thermal transpiration flow in short microchannel was considered for a channel with length-to-height ratio of 5 at Kn_{II}=0.2. To study this effect, the pressure was assumed equal in the two reservoirs, and the temperature drop was set to 300 K. The three cases of temperature distribution are (i) the linear temperature variation along the channel wall (case III-a), (ii) a step-wise temperature variation (case III-b) and (iii) a non-monotonic distribution typical for a radiatively heated nanomembrane Knudsen compressor [18] (case III-c). A non-monotonic wall temperature profile has a maximum of 750 K at one-fourth of the channel length.

The change in the wall temperature distribution significantly impacts the flow velocity (see Fig. 11). Note that only a portion of computational domain is shown to illustrate the details of the flow inside the channel. This impact is noticeably stronger that the one shown in the previous section, and is observed both at the centerline and near the surface.

The influence of wall temperature distributions inside the channel on the centerline temperature profile is illustrated in Fig. 12. The gas temperature generally follows the surface temperature inside the channel, with the end effects being visible even at a distance from the inlet/outlet equal to the channel length. The end effects are somewhat smaller for the stepwise distribution, and largest for the non-monotonic profile.

Figure 13 shows the calculated pressure profiles along the centerline for the above temperature distributions. The qualitative behavior is similar for the linear and stepwise distribution, with pressure larger in the hot part, and smaller in the cold part. The non-monotonic case significantly differs from the first two, since there is no significant pressure minimum in the cold part. Also, there is a pressure increase inside the channel of about 10 percent for the monotonic profile due to the reverse transpiration.

The calculated mass flow rate and flow coefficient Q_T for the three cases are listed in Table 4. The mass flow rate in case of stepwise temperature variation is only slightly lower (by $\approx 3\%$) than for the linear temperature variation. However, the reverse transpiration in the non-monotonic temperature distribution case results in significant degradation of mass throughput (by $\approx 18\%$).

3.4 BGK Model Solution for a Long Microchannel

Results of the validation study of a long channel flow modeling using a BGK model kinetic equation are presented in this section. The flow of nitrogen in a channel with a length-to-height ratio of 30 was calculated for a pressure ratio of 1.5 and a constant temperature of the wall of 300 K. The temperature in the upstream and downstream reservoirs is equal to 300 K. The Knudsen number based on the channel height and the mean free path in the downstream reservoir is 0.05.

The X-component of velocity field is shown in Fig. 14 obtained using three different uniform spatial grids in the BGK solver. The grid dimensions are: (i) 101x51, (ii) 51x26 and (iii) 26x14. The analytical approximate solution[19] of Navier-Stokes equations for a long channel flow with slip boundary conditions is also plotted in Fig.14. The discrete ordinate solution of BGK model kinetic equation with coarser grids results in a lower velocity in the whole computational domain. Note that a similar dependence of results on the number of simulated

particles and cells in the DSMC method was observed [20]. The solution obtained for a 101x51 grid is in excellent agreement with the Navier-Stokes solution.

4 Conclusions

The direct simulation Monte Carlo method and the discrete ordinate method for the solution of the BGK model were used to numerically study rarefied gas flows through two-dimensional finite length capillaries. A wide range of Knudsen numbers was examined, from 0.05 to 75, in the presence of density and/or temperature gradients. The length-to-height ratios varied from 5 to 30. Three different wall temperature distributions were considered, namely, linear, step-wise, and a non-monotonic profile typical for a radiantly heated Knudsen compressor membrane.

For the pressure-driven flow in a short channel with a length-to-height ratios of 5 and 15, the end effects result in the effective elongation of the capillary. The effective elongation increases with the Knudsen number. The flow coefficient is larger for the longer channel due to smaller influence of end effects on the mass flow. The minimum in the flow coefficient, so called Knudsen minimum, is observed at a Knudsen number of about 3 for a channel with L/h=15. The mechanism for the Knudsen minimum in flow conductance is quantitatively explained by using five chemically identical species in DSMC simulations. The computations showed that the Knudsen minimum exists not only for a relatively long channel of L/h=15, but also for a short channel with L/h=5.

The influence of wall temperature distribution on the thermal transpiration flow in a short channel at Kn_{II}=0.2 was considered. The qualitative flow behavior is similar for the linear and stepwise distribution, with pressure larger in the hot part, and smaller in the cold part. The non-monotonic wall temperature distribution case significantly differs from the first two, since there is no significant pressure minimum in the cold part.There is a pressure increase inside the channel of about 10 percent for the monotonic profile due to the reverse transpiration. The mass flow rate in case of stepwise temperature variation is only slightly lower (by 3%) than for the linear temperature variation. However, the reverse transpiration caused by the non-monotonic wall temperature distribution results in significant degradation of mass flow, by about 18%.

The application of the numerical techniques discussed in this paper to detailed investigations and optimizations of microscale thermal creep flows will be extremely valuable. Temperature gradient driven flows are very sensitive to thermal boundary conditions. For practical microdevices it is generally difficult to attain idealized thermal boundary requirements. Thus, numerical methods for reliably estimating the magnitude of the consequences induced by non-ideal conditions are important. The work reported here is a first look at describing practical thermal gradient driven or thermal creep flows.

As an illustration of the usefulness of this approach consider the recent development by Young [5] of a prototype Knudsen Compressor. Radiant energy was used to generate temperature gradients in the carbon doped aerogel membranes that are the active elements in the compressor's pumping stages. Due to finite photon mean free paths in the carbon doped aerogel membranes, the wall temperatures in the membrane's flow passages had a maximum near to, but not at, the exit surface of the membrane. This was the motivation for the calculations reported in Sec. 3.3, with the non-monotonic wall temperature variation of case III-c constructed to mimic the essentials of a membrane in Young's experiments. While the available results are at present both scarce and preliminary, they do validate in this case what was anticipated, and provide useful quantitative estimates of the consequences of the particular wall temperature maximum chosen for the calculations.

5 Acknowledgments

This work has been supported by the Air Force Research Laboratory Propulsion Directorate under Contract No. F04611-99-C-0025. A.A. was supported in part by USC WiSE fellowship. This support is gratefully acknowledged. The authors are thankful to Drs. F.Sharipov and A.M. Alekseenko for helpful discussions of implementation of the discrete ordinate method.

References

[1] M. Knudsen, "Eine Revision der Gleichgewichtsbedingung der Gase. Thermische Molecularstr´omung", *Ann. Phys., Leipzig*, Vol. 31, 1910, pp. 205-229.

[2] Pham-Van-Diep, G., Keeley, P., Muntz, E. P., and Weaver, D. P., "A Micromechanical Knudsen Compressor", In *Rarefied Gas Dynamics*, eds. J. Harvey, G. Lord, Oxford University Press, Oxford, 1995, pp. 715-721.

[3] Vargo, S. E., and Muntz, E. P., "An Evaluation of a Multiple Stage Micromechanical Knudsen Compressor and Vacuum Pump", In *Rarefied Gas Dynamics*, eds. Ching Shen, Peking University Press, Beijing, 1997, pp. 995-1000.

[4] McNamara, S., and Gianchandani, Y. B., "A Micromachined Knudsen Pump for On-Chip Vacuum", *Proceedings of the 12th International Conference on Solid State Sensors, Actuator and Microsystems, Boston, MA*, June 2003, Vol. 2, pp. 1919-1922.

[5] Sharipov, F., and Seleznev, V., "Data on Internal Rarefied Gas Flows", *J. Phys. Chem. Ref. Data*, Vol. 27, No. 3, 1998, p. 657-706.

[6] G. A. Bird, *Molecular Gas Dynamics and Direct Simulation of Rarefied Gas Flows*. Oxford Science Publication, 1994.

[7] M. S. Ivanov, G. N. Markelov, and S. F. Gimelshein, "Statistical simulation of reactive rarefied flows: numerical approach and applications," *AIAA Paper 98-2669*, June 1998.

[8] M. S. Ivanov, S. V. Rogasinsky, "Analysis of numerical techniques of the direct simulation Monte Carlo method in the rarefied gas dynamics," *Sov. J. Numer. Anal. Math. Modeling* Vol. 2, No. 6, 1988, pp. 453-465.

[9] K. Koura, H. Matsumoto, "Variable soft sphere molecular model for inverse-power-law of Lennard-Jones potential," *Phys. Fluids A*, Vol. 3, No. 10, 1991, pp. 2459-2465.

[10] C. Borgnakke, and P. S. Larsen, "Statistical collision model for Monte Carlo simulation of polyatomic gas mixture," *J. Comp. Phys.* 18:405-420, 1975.

[11] Cai, C., Boyd, I. D., Fan, J., and Candler, G. V., "Direct Simulation Methods for Low-Speed Microchannel Flow", *J. Thermophysics and Heat Transfer*, Vol. 14, No. 3, 2000, pp. 368-378.

[12] Bhatnagar, P.L, Gross, E.P., and Krook, M., "A Model for Collision Processes in Gases. I. Small Amplitude Processes in Charged and Neutral One-Component Systems", Phys. Rev., Vol. 94, No. 3, 1954, pp. 511-525.

[13] Chung, C.H., and Wereley, S., "Analysis of Gas Flows in Microchannels with Small Pressure Difference", *AIAA Paper 2003-861*, January 2003.

[14] Shizgal, B., "A Gaussian Quadrature Procedure for Use in the Solution of the Boltzmann Equation and Related Problems", *J. Comp. Physics*, Vol. 41, 1981, pp. 309-328.

[15] Loyalka, S. K., "Kinetic theory of thermal transpiration and mechanocaloric effect. II", *J. Chem. Phys.*, Vol. 63, No. 9, 1975, pp. 4054-4060.

[16] Berman, A. S., "Free Molecule Transmission Probabilities", *J. Appl. Phys.*, Vol. 36, No. 10, 1965, p. 3356.

[17] Pollard W.G., Present, R.D. "On Gaseous Self-Diffusion in Long Capillary Tubes," *Phys. Review*, Vol. 73, 1948, pp. 762-774.

[18] Young, M., *Investigation of Several Important Phenomena Associated With the Development of Knudsen Compressors*, Ph.D. Thesis, University of Southern California, June 2004.

[19] Arkilic, E. B., Schmidt, M. A., and Breuer, K. S., "Gaseous Slip Flow in Long Microchannels", *J. of MEMS*, Vol. 6, No. 2, June 1997, pp. 167-178.

[20] Alexeenko, A., Gimelshein, S.F., and Levin, D.A., "Reconsideration of Flows through Constriction Microchannels using the DSMC Method", *AIAA Paper 2003-4009*, June 2003.

Table 1: Summary of cases considered

Flow Conditions	Designation
Pressure-Driven Flow in Short Microchannels	
L/h=5, N_2, $T_I = T_{II}$ = 300 K, $\frac{p_I}{p_{II}}$=1.5	
Kn_{II}=50	*case I-a*
Kn_{II}=3	*case I-b*
Kn_{II}=1	*case I-c*
Kn_{II}=0.2	*case I-d*
Kn_{II}=0.05	*case I-e*
Pressure and Temperature-Driven Flow	
L/h=5, N_2, T_I=600 K, T_{II}=300 K, $\frac{p_I}{p_{II}}$=1.5	
Kn_{II}=50	*case II-a*
Kn_{II}=3	*case II-b*
Kn_{II}=1	*case II-c*
Kn_{II}=0.2	*case II-d*
Kn_{II}=0.05	*case II-e*
Effect of Wall Temperature Distribution	
L/h=5, Kn_{II}=0.2, N_2, T_I=600 K, T_{II}=300 K, $\frac{p_I}{p_{II}}$=1.0	
linear	*case III-a*
step	*case III-b*
non-monotonic	*case III-c*

Table 2: Average exit mole fraction and mass flow of different species for Kn_{II}=75.

Species	Fraction, %	m, kg/s
1	1.1	$3.56{\cdot}10^{-9}$
2	3.5	$8.14{\cdot}10^{-9}$
3	6.2	$1.438{\cdot}10^{-8}$
4	46.2	$-9.58{\cdot}10^{-8}$
5	43.1	$7.84{\cdot}10^{-8}$
Total	100	$4.44{\cdot}10^{-9}$

Table 3: Average exit mole fraction and mass flow of different species for Kn_{II}=1.5.

Species	Fraction, %	m, kg/s
1	0	0
2	0	0
3	8.9	$7.22{\cdot}10^{-7}$
4	35.3	$-3.88{\cdot}10^{-6}$
5	55.1	$3.532{\cdot}10^{-6}$
Total	100	$3.74{\cdot}10^{-7}$

Table 4: Calculated mass flow rate and flow coefficients for pressure-driven flow in short channel.

Case	$\dot{m}$ (kg/s)	Q_P	$\frac{\dot{m}}{\Delta p} \times 10^7$ ($kg/s \cdot Pa$)
I-a	$0.261{\times}10^{-7}$	1.00	4.76
I-b	$0.429{\times}10^{-6}$	0.989	4.69
I-c	$0.134{\times}10^{-5}$	1.03	4.88
I-d	$0.936\mathrm{E}{\times}10^{-5}$	1.44	6.82
I-e	$0.746{\times}10^{-4}$	2.87	13.6
II-a (lin)	$0.119{\times}10^{-7}$	0.533	2.17
II-a (step)	$0.119{\times}10^{-7}$	0.533	2.17
II-b (lin)	$0.229{\times}10^{-6}$	0.615	2.5
II-b (step)	$0.229{\times}10^{-6}$	0.615	2.5
II-c (lin)	$0.812{\times}10^{-6}$	0.727	2.96
II-c (step)	$0.824{\times}10^{-6}$	0.738	3.0
II-d (lin)	$0.672{\times}10^{-5}$	1.20	4.90
II-d (step)	$0.677{\times}10^{-5}$	1.21	4.93
II-e (lin)	$0.555{\times}10^{-4}$	2.49	10.11
II-e (step)	$0.554{\times}10^{-4}$	2.48	10.09

Table 5: Calculated mass flow rate and flow coefficient for temperature-driven flow in short channel.

Case	$\dot{m}$ (kg/s)	Q_T
III-a	1.580E-6	0.1189
III-b	1.532E-6	0.1153
III-c	1.292E-6	0.0972

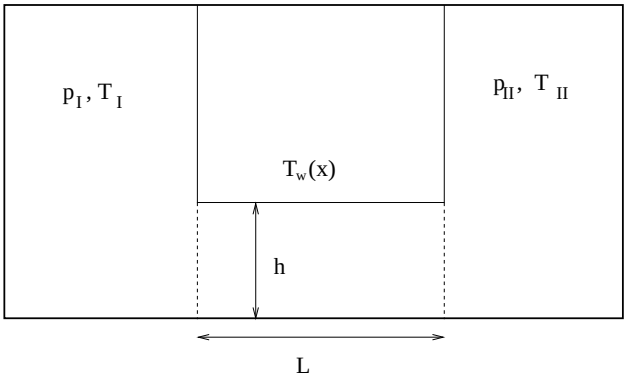

Figure 1: Schematic of the problem and notations.

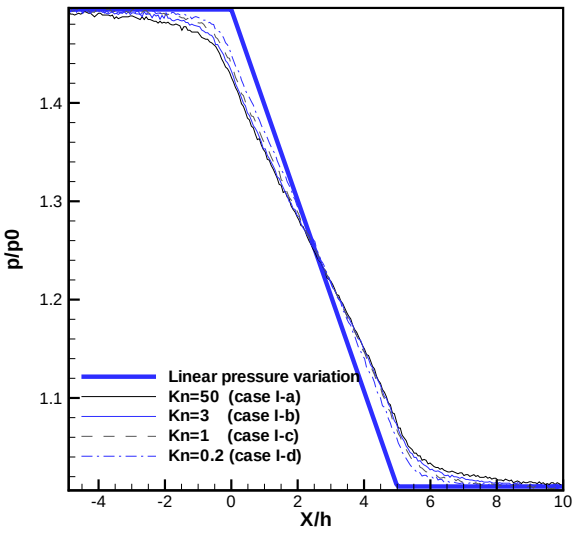

Figure 2: Normalized pressure along X-axis.

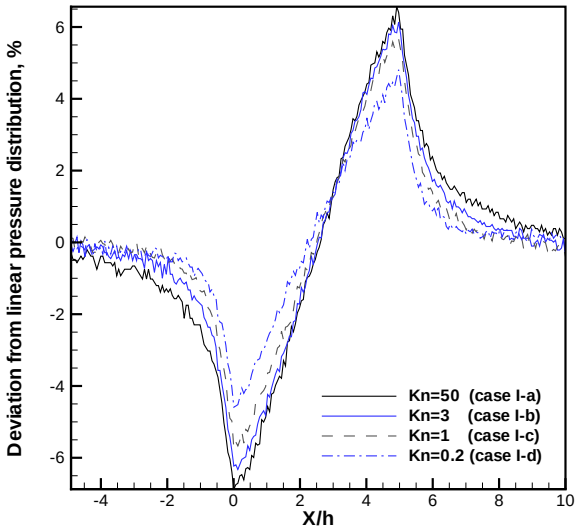

Figure 3: Deviation from the linear pressure distribution along X-axis.

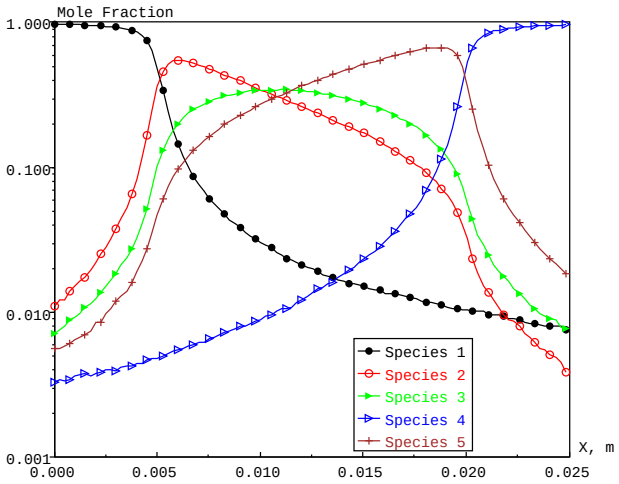

Figure 5: Distribution of the mole fraction of different species along the flow centerline for Kn_{II}=75

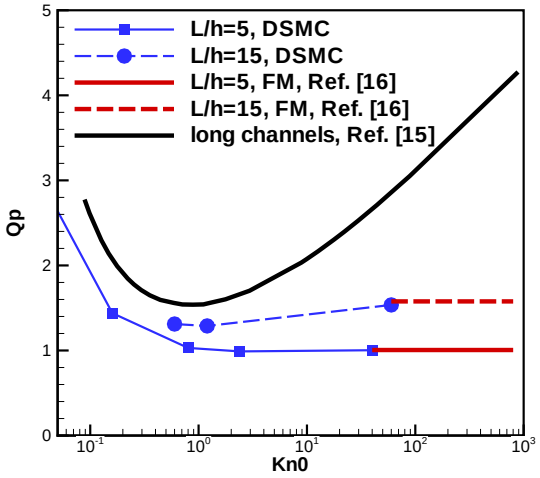

Figure 4: Flow coefficient Q_p.

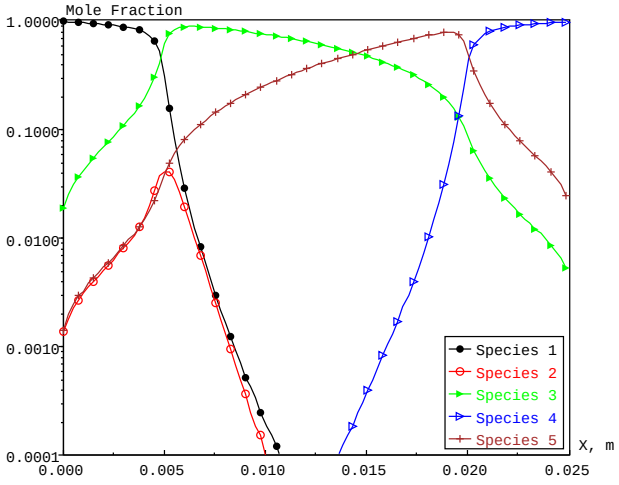

Figure 6: Distribution of the mole fraction of different species along the flow centerline for Kn_{II}=1.5

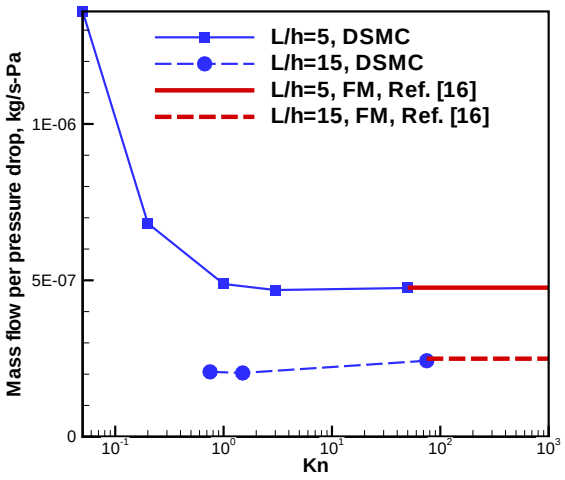

Figure 7: Mass flow rate per pressure drop.

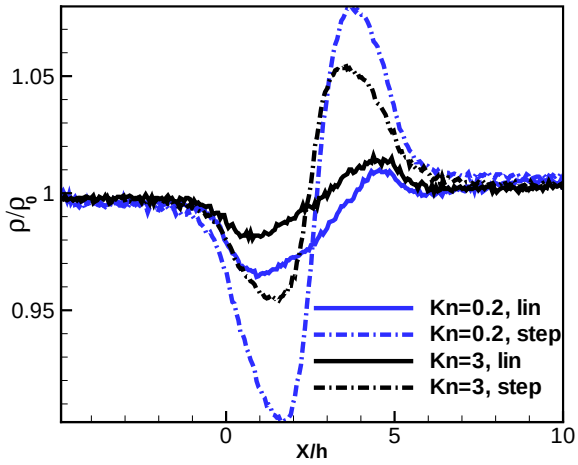

Figure 9: Normalized density profile along the channel for different temperature variations and Knudsen numbers.

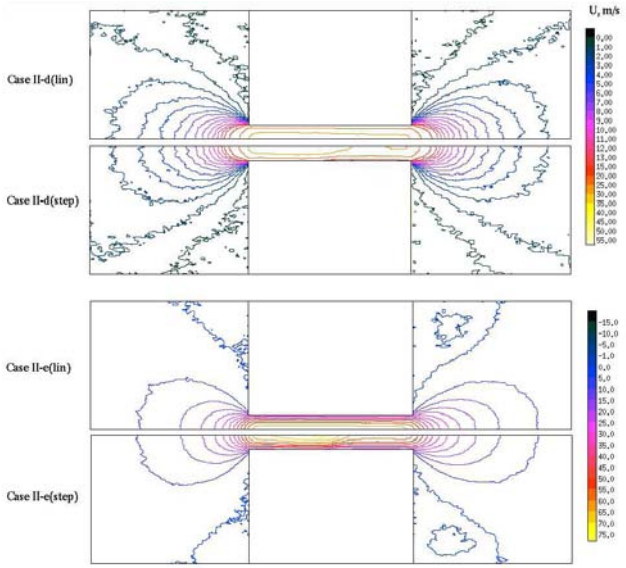

Figure 8: X-component of velocity field for Cases II-d and II-e.

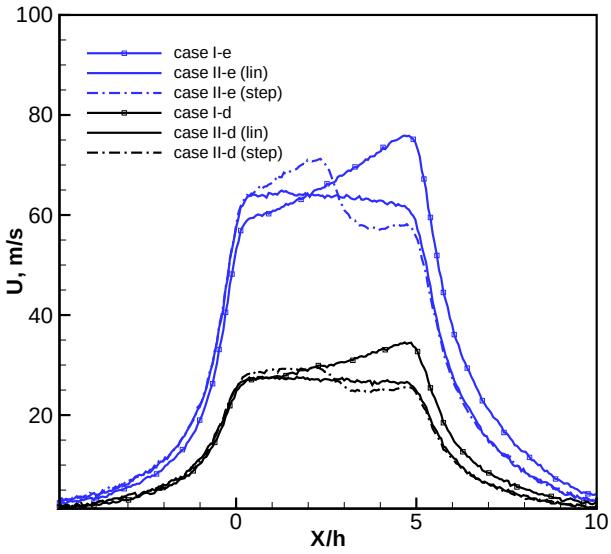

Figure 10: X-component of velocity profile along the channel for different temperature distributions and Knudsen numbers.

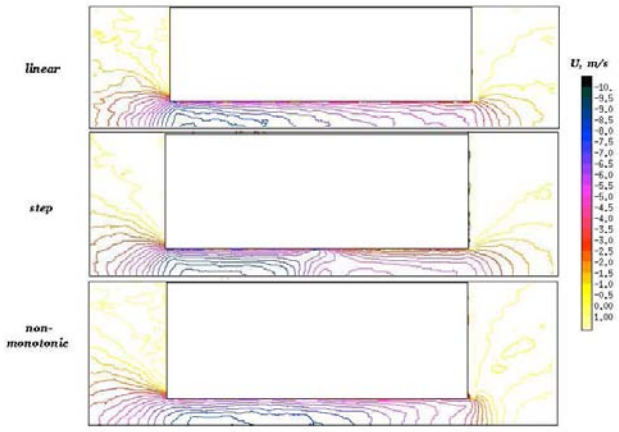

Figure 11: X-component of velocity field, Kn_{II}=0.2, L/h=5 for different temperature variations.

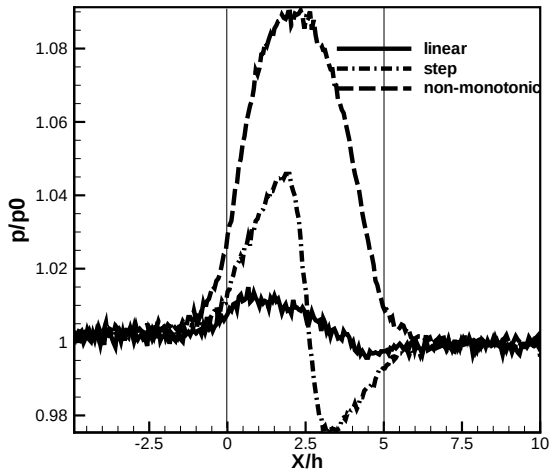

Figure 13: Pressure distribution along the channel, Kn_{II}=0.2, L/h=5 for different temperature variations.

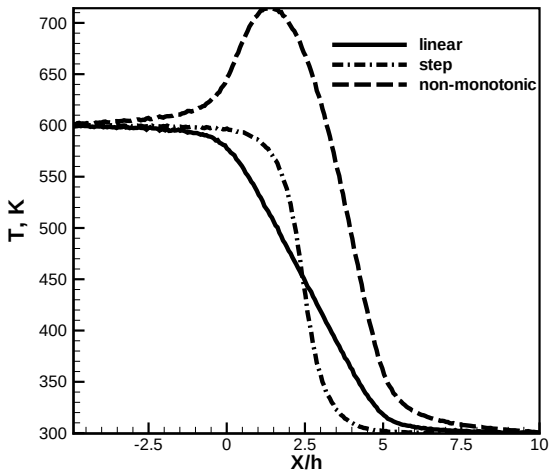

Figure 12: Temperature distribution along the channel, Kn_{II}=0.2, L/h=5 for different temperature variations.

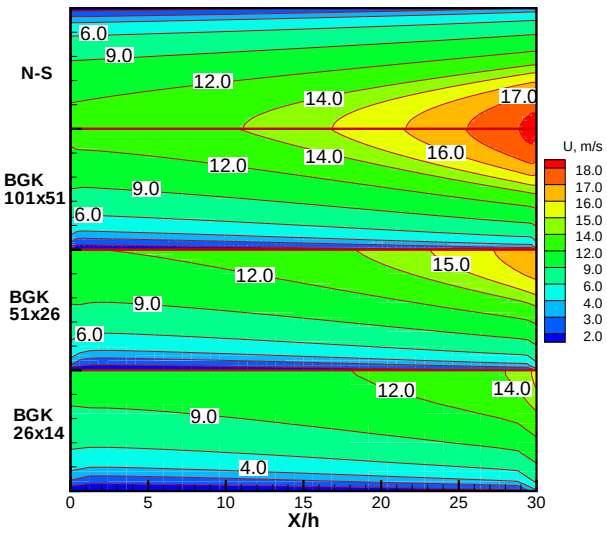

Figure 14: X-component of velocity field, Kn_{II}=0.05, L/h=30.